Journal of Inflammation Research

Dovepress
open access to scientific and medical research

Open Access Full Text Article

ORIGINAL RESEARCH

Circ_0008146 Exacerbates Ferroptosis via Regulating the miR-342-5p/ACSL4 Axis After Cerebral Ischemic/Reperfusion

Cai-Dong Liu[1,2,*], Qiang Peng[3,*], Shi-Yao Wang[3,*], Yang Deng[2], Zhong-Yuan Li[3], Zhao-Han Xu[3], Liang Wu[3], Ying-Dong Zhang[2,3], Rui Duan[3]

[1]Department of Laboratory Medicine, Nanjing First Hospital, China Pharmaceutical University, Nanjing, Jiangsu, 210006, People's Republic of China; [2]School of Basic Medicine and Clinical Pharmacy, China Pharmaceutical University, Nanjing, Jiangsu, 210006, People's Republic of China; [3]Department of Neurology, Nanjing First Hospital, Nanjing Medical University, Nanjing, Jiangsu, 210006, People's Republic of China

*These authors contributed equally to this work

Correspondence: Ying-Dong Zhang; Rui Duan, Department of Neurology, Nanjing First Hospital, Nanjing Medical University, No. 68, Changle Road, Nanjing, Jiangsu, People's Republic of China, Email zhangyingdong@njmu.edu.cn; duanruicpu@163.com

Purpose: Acute ischemic stroke (AIS) has seriously threatened people's health worldwide and there is an urge need for early diagnosis and effective treatment of AIS. This research intended to clarify the regulatory role of circ_0008146/miR-342-5p/ACSL4 axis in AIS.

Methods: High-throughput small RNA sequencing analysis was adapted to identify differentially expressed miRNAs between the AIS and control group. The circ_0008146, miR-342-5p, and ACSL4 levels were detected by qRT-PCR. Middle cerebral artery occlusion/reperfusion (MCAO/R) models were constructed in C57BL/6J mice. Assay kits were used to determine Fe^{2+} levels and a battery of oxidative stress and lipid peroxidation indicators, including ROS, MDA, LPO, SOD and GSH/GSSG ratio. The protein levels of ACSL4 were measured by Western blot. The behavioral function was assessed using neurobehavioral tests. TTC staining was employed to visualize infarction size. Nissl staining was adapted to detect histopathological changes. Receiver operating characteristic curve and correlation analysis were applied to investigate the clinical value and association of miR-342-5p and ACSL4.

Results: A total of 44 AIS patients and 49 healthy controls were enrolled in our study. The small RNA sequencing unveiled a significant decrease in miR-342-5p levels in AIS patients. MiR-342-5p inhibited oxidative stress and RSL3-induced ferroptosis after cerebral ischemic/reperfusion injury in vivo by targeting ferroptosis-related gene ACSL4. Circ_0008146 acted as a sponge of miR-342-5p, and overexpression of circ_0008146 increased neurological deficits and brain injury in mice. Circ_0008146 contributed to ferroptosis in cerebral infarction via sponging miR-342-5p to regulate ACSL4. Plasma miR-342-5p and ACSL4 demonstrated significant correlation and good diagnostic value for AIS patients.

Conclusion: This study provides the first in vivo evidence to show that circ_0008146 exacerbates neuronal ferroptosis after AIS via the miR-342-5p/ACSL4 axis. Furthermore, miR-342-5p/ACSL4 axis holds promise as a viable therapeutic target and practical biomarkers for AIS patients.

Keywords: ischemic stroke, miRNA, circRNA, ferroptosis, biomarker

Introduction

Acute ischemic stroke (AIS), a critical and severe disorder, is the result of a sudden decrease in cerebral circulation.[1] Featured with high incidence, mutilation and death rate, AIS has threatened people's health seriously.[2] Common pathological changes in the brain include the accumulation of toxins, global brain inflammation, cellular energy depletion and cell necrosis.[3,4] For AIS patients, intravenous infusion of alteplase remains the most recommended as well as the sole FDA-approved treatment.[5,6] However, the effectiveness of thrombolytic therapy is constrained by a short time frame, in addition to potential side effects.[7] At the same time, few neurotherapeutic drugs are clinically available to treat more

Received: 27 May 2024
Accepted: 16 July 2024
Published: 23 July 2024

severe secondary brain injury, cerebral ischemia/reperfusion injury. This damage, in some cases, might be caused by the prompt blood-supply recovery as the main treatment for ischemic stroke.[8] Therefore, there is an urgency for further exploration and new therapeutic approaches to AIS.

Iron is widely distributed and serves as a vital participant in numerous bioprocesses in the brain.[9] Individuals exhibiting heightened serum ferritin levels typically face a more devastating prognosis within 24 h of cerebral ischemia.[10] Ferroptosis is defined as a type of non-apoptotic cell death, usually distinguished by the iron-dependent buildup of lipid reactive oxygen species (ROS).[11–13] Both iron metabolism and lipid peroxidation signaling are now considered as primary factors of ferroptosis.[12] Long-chain acyl-CoA synthetase 4 (ACSL4), a member of the ACSL family, is capable of initiating lipid peroxidation and prone to inducing ferroptosis.[14] ACSL4 and ferroptosis are closely associated with ischemia/reperfusion injury, and knockdown of ACSL4 or inhibition of ferroptosis have shown promising therapeutic potential.[15] However, the specific regulatory mechanisms underlying this process remain unclear.

MicroRNAs (miRNAs) belong to a subgroup of small non-coding RNA, playing an essential role in regulating gene expression.[16] They hold relevant competencies for modulating the level of specific gene through influencing stability of mRNA of interest or suppressing translational efficiency.[17] These biomolecules can be detected in circulation and have been extensively explored as putative indicators for predicting, diagnosing and prognosing various physiological conditions.[18] Previous studies have elucidated the biological functions of miR-342-5p in various conditions. For example, the overexpression of miR-342-5p in HER2+ breast cancer cells significantly impacted HER2 downstream signaling, cell motility, and mitochondrial stability.[19] It was observed that miR-342-5p is upregulated in transgenic AD mice and speculated that its alteration may contribute to AD axonopathy by downregulating AnkG.[20] MiR-342-5p in exosomes was also reported to exert anti-apoptotic and cardioprotective effects by targeting caspase 9, an apoptosis-inducing factor.[21] Nevertheless, there is limited research on the relationship between miR-342-5p and AIS.

Featured with a covalently closed loop structure, circular RNAs (circRNAs) are available to evade degradation caused by nuclease.[22] Researchers have discovered plenty of endogenous circRNAs in mammalian cells, with some demonstrating high abundance and evolutionarily conservation.[23,24] Studies also have demonstrated that certain exonic circRNAs can function as miRNA sponges or modulate the content of linear protein-encoding RNA products by "mRNA trap" mechanisms.[23,25] These mechanisms allow circRNAs to exert control over gene expression and potentially affect various cellular processes.[23] For example, there were studies indicating that miR-197 could be sponged by circ_0001017 and regulate the cancer-related gene RHOB, which was helpful in ameliorating gastric cancer progression.[26] Another example is that CircEPS15 acts as a sponge of miR-24-3p to regulate mitophagy gene PINK1, enhancing neuronal protection in Parkinson's disease.[27] Similarly, CircZXDC can absorb miR-125a-3p, leading to an upregulation of ABCC6 expression, which triggers endoplasmic reticulum stress and hence contributes to the thickening of the intima in Moyamoya disease vessels.[28] Previous study also shown the regulatory role of circRNA-miRNA-mRNA network on ferroptosis in stroke patients.[29] Even so, the specific contribution of circRNAs in AIS is still unclear.

In the current study, we identified miR-342-5p as downregulated in ischemic stroke patients by small RNA sequencing, and discovered the regulatory effect of circ_0008146/miR-342-5p/ACSL4 axis on ferroptosis by in vivo stroke models. Finally, we verified the expression relationship between miR-342-5p and ACSL4 in clinical samples, and provided a new potential treatment strategy for AIS.

Materials and Methods

Study Population and Samples

Blood samples were obtained from healthy controls and AIS patients who visited Nanjing First Hospital between January 2021 and September 2023. The AIS group were enrolled according to the following inclusion: (1) over 18 years of age; (2) admitted within 48 h after symptom onset. The symptom onset was defined as the time new neurological deficits appear. For wake-up stroke patients, it was defined as the last known normal time;[30,31] (3) confirmed by imaging tests utilizing MRI or CT. Subjects were excluded if: (1) severe comorbidities including the heart, liver, kidney and other vital organ failure or insufficiency; (2) a history of intracranial hemorrhage or tumor; (3) unsigned informed consent. The blood samples of AIS patients were collected within 24 h of admission to the hospital. After centrifugation at 500 g for

a quarter hour, samples were obtained and then stored at −80 °C for future use. The control group consisted of individuals who visited our hospital seeking physical examinations. Blood samples were drawn from them in a similar manner to the AIS group. This study was in full compliance with the Declaration of Helsinki and was approved by the Ethics Committee of Nanjing First Hospital, Nanjing Medical University (No. KY20211011-05). All study participants provided written informed consent before enrollment in the study.

Small RNA Sequencing

Blood samples from two AIS patients and two normal individuals were collected for RNA sequencing. Firstly, total RNA was isolated from the aforementioned collected plasma with miRNeasy Mini Kit (Qiagen, Hilden, NRW, Germany). Small RNAs ranging from 18 to 30 nucleotides were obtained through gel electrophoresis from total RNA. Following that, 3' and 5' adapters were successively added. The RNAs with the adapters added were then reverse transcribed, and the cDNA products ranging from 140 to 160 base pairs were obtained to construct the cDNA library. Then RNAs were sequenced on the Illumina HiSeqTM 2500 by Gene Denovo Biotechnology Co. (Guangzhou, China). All the obtained data were processed normally, and the differentially expressed miRNAs were screened as per the criterion $|\log2\ (FC)| > 1$ and $P<0.05$. In addition, the sequencing results have been stored in the Gene Expression Omnibus (GSE254322).

Quantitative Real-Time Polymerase Chain Reaction (qRT-PCR) Analysis

Total RNA in the collected plasma from AIS patients and controls was extracted with miRNeasy Mini Kit (Qiagen, Hilden, NRW, Germany). Total RNA in mouse brain tissues was extracted with Trizol reagent (Invitrogen, CA, USA) at 24 h after MCAO/R modeling. Then, the content of extracted RNA was assessed using a Nanodrop 2000 spectrophotometer (Thermo Fisher Scientific, USA). Next, taking advantage of a reverse transcription kit supported by Takara Bio, the extracted RNA was reverse transcribed, resulting in the generation of ideal cDNA. The qRT-PCR reaction was conducted by the ABI7500 type sequence detection system (7500, ABI, USA) using the SYBR-Green method, and each well's cycle threshold (CT) was recorded. β-actin (for circRNA) or U6 (for miRNA) served as the housekeeping gene, as appropriate. Lastly, the relative expressions of the genes were assessed by the $2^{-\Delta\Delta Ct}$ approach. The primers have been shown in Supplementary Table 1.

Functional Enrichment Analysis

Potential functions and signal paths of target genes for hsa-miR-342-5p were predicted by leveraging Gene Ontology (GO) enrichment analysis or Kyoto Encyclopedia of Genes and Genomes (KEGG) path analysis approaches using clusterProfiler (version 3.11) of R package. The biological processes, cellular components, and molecular functions of miR-342-5p target genes were identified in GO enrichment analysis. The significantly enriched Top 30 pathways based on FDR value were demonstrated in KEGG enrichment analysis.

Animals

C57BL/6J male mice (8–10 weeks, 20–25g) were provided by Beijing Zhishan Co., Ltd (Beijing, China). All of them were housed in a regulated environment with 60 ± 5% humidity and a temperature of 23 ± 1°C, under a daily 12-hour light and dark phase. Food and water were consumed ad libitum. Mice were randomly divided into each group. A minimum of six mice were examined at every time point, and the investigator was concealed from the group assignment. This study was approved by the Laboratory Animal Ethics Committee of Nanjing First Hospital, Nanjing Medical University (No. DWSY-23146450). The experimental protocol was conducted in accordance with the Guide for the Care and Use of Laboratory Animals of the National Institutes of Health.

Middle Cerebral Artery Occlusion/Reperfusion (MCAO/R) Model

MCAO/R model, a well-established animal model for AIS, was constructed as described previously.[32,33] First of all, mouse was treated with 2% isoflurane in oxygen (RWD Life Science, Shenzhen, China) for anesthetization. After confirming anesthetic depth, a midline neck incision was made. Then, the internal, external and common carotid arteries were separated through blunt dissection. Following the ligation of the external carotid, a silicon-coated monofilament

(Cinontech, Beijing, China) was carefully inserted through the internal carotid artery. When feeling slight resistance, stop the insertion of the monofilament. One hour later, monofilament was gently pulled down. The procedure was true to the Sham group except for suture insertion. At last, the post-operation mice were kept on a heating pad (37 ± 0.5 °C).

Reactive Oxygen Species (ROS), Malondialdehyde (MDA) and Lipid Peroxidation (LPO) Levels

At 24 h after MCAO/R modeling, cortical tissue samples were collected from the operation groups, along with the corresponding area from the Sham group. For measurement of ROS, the samples were washed with PBS and prepared into a single-cell suspension. For measurement of MDA and LPO, the samples were homogenized with PBS. The content of ROS (#E004), MDA (#A003) and LPO (#A106) was assessed using the corresponding assay kits, all of which were provided by Nanjing Jiancheng Bioengineering Institute. Special instructions were obtained in advance, and procedures were carried out following the manufacturers' protocols.

Superoxide Dismutase (SOD) Activity and Total Glutathione/Oxidized Glutathione (GSH/GSSG) Ratio

At 24 h after MCAO/R modeling, sample preparation was carried out as described above. Briefly, the samples were homogenized with PBS, then centrifuged to collect the supernatant. SOD activity (#A001), as well as GSH/GSSG ratio (#A061), were detected using the corresponding SOD Assay Kit and GSH/GSSG Assay Kit, all of which were provided by Nanjing Jiancheng Bioengineering Institute. Special instructions were obtained in advance, and procedures were carried out following the manufacturers' protocols.

Luciferase Reporter Assays

TargetScan 7.2 online prediction website (https://www.targetscan.org/vert_72/) was used to predict consequential pairing of 3'-UTR sequence of ACSL4 and miR-342-5p. RNAhybird (https://bibiserv.cebitec.uni-bielefeld.de/rnahybrid) was performed to predict the potential binding sites of miR-342-5p in circ_0008146. The WT or Mut of ACSL4 3'-UTR or circ_0008146 luciferase reporter constructs were co-transfected into HEK 293T cells along with miR-342-5p mimic or NC mimic using Lipofectamine 2000 as the transfection agent, respectively. Waiting for 2 d, harvested cells were examined using dual-luciferase reporter assay system supported by Promega.

Treatment with RAS-Selective Lethal 3 (RSL3)

RSL3 was administered as described previously.[34] RSL3 has been widely reported to be an inducer of ferroptosis.[35] Aim to assess the effect of miR-342-5p on ferroptosis under ischemic and secondary reperfusion conditions, the mice were randomly divided into 4 groups, consisting of the Sham group, MCAO/R group, MCAO/R + RSL3 + NC mimic group, and MCAO/R + RSL3 + miR-342-5p mimic group. RSL3 (S8155, Selleck, Houston, TX, USA), dissolved in the solvent dimethylsulfoxide (DMSO), was intraperitoneally injected into the mice in the later 2 groups at a dose of 30 mg/kg within 24 h before the MCAO/R operation.

Lateral Intracerebroventricular Injection

The LV-circ_0008146 and the negative control (NC) vector were supported by Genechem Company (Shanghai, China). The miR-342-5p mimics and NC mimics were obtained from GenePharma Company (Shanghai, China). At 3 days before MCAO/R operation, mice were anesthetized, and pedal reflexes were checked to confirm successful anesthesia. After shaving and disinfecting the surgical area, mice were fixed on a stereotaxic device (RWD Life Science, Shenzhen, China). Anterior fontanelle was considered as a reference point to pinpoint the right ventricle in mice (anteroposterior (AP), −0.5 mm; mediolateral (ML), −1.0 mm; dorsoventral (DV), −3.0 mm), where lentiviral vectors and miR-342-5p mimics or NC mimics were injected at a rate of 0.2 μL/min using a microsyringe (Hamilton, Nevada, USA). The microsyringe was left in place for a duration of 20 min before being withdrawn. Following the removal of the needle, bone wax was applied to seal the burr hole, and the incision was sutured closed, allowing the mice to recover.

Western Blot

At 24 h after MCAO/R modeling, the mouse brain tissues were collected. Firstly, the brain tissues were dissected using RIPA lysis buffer (Thermo Fisher Scientific, USA) on ice. Secondly, above samples were quantified using BCA protein assay kit (Thermo Fisher Scientific, USA). Thirdly, 30–40 μg protein was loaded per sample into wells of 10% sodium dodecyl sulfate-polyacrylamide gel electrophoresis (SDS-PAGE) gels, along with 5 μL PageRuler Prestained Protein Ladder (#26617, Thermo Fisher Scientific, USA). Later, the gels were run in 2 stages (stage 1: 80 V, 30 min; stage 2: 120 V, 60 min). Following electrophoresis, the proteins were transferred onto advanced activated polyvinylidene fluoride (PVDF) membranes (Merck Group, Darmstadt, HE, Germany). Subsequently, above membranes were blocked with 5% skim milk (BD, MD, USA) for 1 h at room temperature. Next, the membranes were placed on a rocker and incubated overnight at 4 °C with the diluted primary antibodies: anti-ACSL4 antibody (1:10,000, #ab155282, Abcam) and anti-β-actin antibody (1:1000, #4970, Cell Signaling Technology). Afterwards, the membranes were rinsed 3 times and then incubated on a rocker with diluted anti-rabbit secondary antibody (1:5000, #7074, Cell Signaling Technology) at room temperature for 2 h. Finally, the membranes underwent three additional washes before being imaged by Enhanced Chemiluminescence Plus kit (Thermos Fish Scientific, USA). Densitometric analysis was performed using ImageJ software (National Institutes of Health, Bethesda, MD, USA). Each experimental sample was normalized to β-actin.

Iron Assay

At 24 h after MCAO/R modeling, sample preparation was carried out as described above for ferrous iron assay using the iron assay kit (Abcam, Cambridge, UK). Samples preparation and assay procedures strictly followed the recommendations. In the end, the output was assessed on a colorimetric microplate reader (OD 593 nm).

Neurobehavioral Tests

The neurobehavioral tests include the modified Neurologic Severity Score (mNSS), rotarod test, and corner test, all of which were performed before MCAO/R operation and on days 1, 3, and 7 after MCAO/R operation to evaluate neurobehavioral functions. Behavioral analyses were performed by personnel who were unaware of the study groups.

mNSS Assessment

All mice were rated by mNSS (scores 0–14) regarding the neurobehavior function and classified into slight injury (scores 1–4), moderate injury (5–9), and serious injury (10–14). This assessment encompassed motor, reflex and balance tests. The higher the score, the more severe the injury.

Corner Test

The corner test was used to evaluate sensorimotor asymmetry. Two 30cm × 20cm cardboards were positioned at a 30° angle with a narrow gap. The mice were positioned in the middle of the two cardboards, allowing their vibrissae on both sides to be stimulated when they entered the corner. The direction in which they turn back was recorded. Typically, the probability of turning in either direction was equal. However, following MCAO/R that resulted in contralateral limb deficits, mice tended to use their ipsilateral limbs (right side) to turn back. A stronger preference for one side indicates a more severe ischemic stroke outcome.

Rotarod Test

The rotarod test was utilized to test the overall motor performance. Mice were placed on a rotating rod and attempted to stay on it rather than falling onto a platform below. The speed progressively rose from 4 to 40 rpm over a 5-minute period. The shorter the duration, the poorer the motor function. The duration they stayed on the accelerating rotating rod was recorded.

2,3,5-Triphenyltetrazolium Chloride (TTC) Staining

TTC staining was adapted to measure cerebral infarction size. At 7 days after MCAO/R modeling, the mouse brains were gently sectioned into six pieces and immersed directly in 12-well plates containing the prepared TTC staining solution (Sigma-Aldrich, St. Louis, MO, USA). The plates were then incubated away from light in a 37 °C water bath for 0.5

h and subsequently fixed with 4% paraformaldehyde (Biosharp, Beijing, China). In the end, ImageJ (National Institutes of Health, Bethesda, MD, USA) was employed to process and analyze specific images, which contained normal tissue (dark red regions) and infarcted areas (white regions).

Nissl Staining

At 7 days after MCAO/R modeling, the mice were anesthetized and the specimen were obtained. 200 mL of normal saline and 4% paraformaldehyde (Biosharp, Beijing, China) was successively injected into the heart of the mice in each group. Afterward, the mouse brains were harvested, dehydrated, and embedded in paraffin. Subsequently, paraffin blocks were divided into 6–8 μm slices. Later, the Nissl staining of the mouse brain slices was performed following the manufacturer's instructions using Nissl staining kit (Solarbio, Nanjing, China). Briefly, the slices were sequentially submerged in xylene, anhydrous ethanol, 95% ethanol, 80% ethanol, 70% ethanol, and double distilled water. Subsequently, the slices were stained with cresyl violet stain. Finally, the aforementioned dehydration steps were repeated in reverse order. The morphology of the ischemia-reperfusion area in the right cortex was examined under an Olympus microscope (Olympus, Tokyo, Japan).

Statistical Analysis

GraphPad prism 8.0 (GraphPad Software, Inc., La Jolla, CA, USA) was utilized for all statistical analyses. Data are shown as mean ± standard deviation (SD). Statistical analysis included Student's *t*-test (for two groups) or one-way ANOVA (for three or more groups) followed by Tukey's post hoc test. Neurobehavioral tests were analyzed using two-way repeated-measures ANOVA followed by Tukey's post hoc test. Receiver operating characteristic (ROC) curve was used to assess the diagnosis value of miR-342-5p and ACSL4 for AIS. The correlation between miR-342-5p and ACSL4 in AIS patients was analyzed by Pearson correlation coefficient. $P < 0.05$ was considered statistically significant.

Results

MiR-342-5p Was Markedly Reduced in the Plasma of AIS Participants

To investigate the involvement of miRNAs in AIS patients, we initially performed high-throughput small RNA sequencing in the plasma of 2 AIS patients and 2 healthy controls. Subsequently, 21 differentially expressed miRNAs (DEmiRNAs) were screened as per the criterion $|\log2\ (FC)| > 1$ and $P<0.05$ (Figure 1A), including 10 downregulated miRNAs and 11 upregulated miRNAs in AIS patients. Considering the potential heterogeneity of clinical samples, we focused on 6 human-mouse homologous miRNAs and further validated their expression in 10 healthy controls and 10 AIS patients. The results revealed a significant alteration in expression levels of 5 miRNAs in AIS patients. Notably, hsa-miR-342-5p exhibited pronounced downregulation (Figure 1B). The GO and KEGG functional enrichment analysis demonstrated that miR-342-5p were involved in multiple stroke-associated activities and signaling pathways, including the MAPK signaling pathway, mitochondrial autophagy, ferroptosis, apoptosis, etc. (Figure 1C and D) Hence, miR-342-5p was selected for further study.

MiR-342-5p Inhibited Oxidative Stress After Cerebral Ischemic/Reperfusion in Mice

It is reported that miR-342-5p reduces the volume of cerebral infarction and relieves the neurological function deficits in vivo.[36] Moreover, substantial evidence suggests that oxidative stress is detrimental in ischemic and reperfusion,[37] which may worsen neuronal damage and result in severe functional deficits.[38] It is known that inhibiting oxidative stress could be an effective approach to alleviate cerebral ischemic/reperfusion injury.[39,40] Hence, we speculated that miR-342-5p may have an effect on oxidative stress. We injected miR-342-5p mimics or NC mimics into the MCAO/R models and miR-342-5p was successfully overexpressed in the brain tissues (Figure 2A). Then, we measured multiple indicators including the levels of ROS, MDA, LPO, SOD and GSH/GSSG, aiming to determine the impact of miR-342-5p on oxidative stress. As expected, compared to the Sham group, the MCAO/R group presented a considerable increase in ROS, MDA and LPO. Besides, the administration of the miR-342-5p mimic effectively reduced aforementioned indicators, suggesting its potential in alleviating oxidative stress (Figure 2B-D). Similarly, the MCAO/R group showed

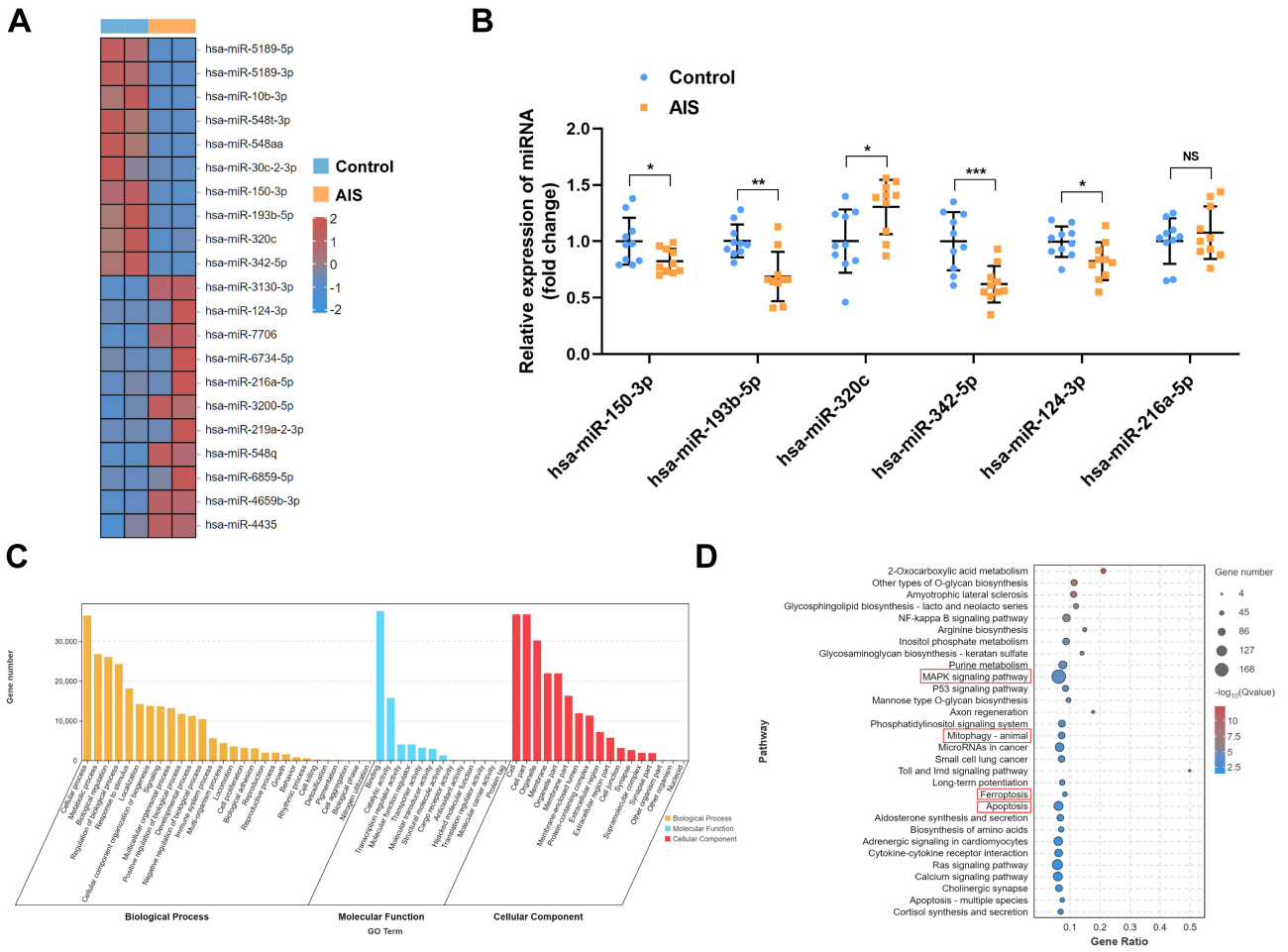

Figure 1 MiR-342-5p was significantly reduced in the plasma of AIS patients. (**A**) Heatmap illustrating the differentially expressed miRNAs (DEmiRNAs) in AIS patients and control subjects by high-throughput sequencing. Red scale: higher expression. Blue scale: lower expression (n = 2 per group). (**B**) Validation of selected human-mouse homologous DEmiRNAs in the plasma from AIS patients and control subjects by qRT-PCR analysis (n = 10 per group). (**C** and **D**) GO and KEGG enrichment analysis of the target genes of hsa-miR-342-5p. Results were expressed as mean ± SD. NS: not significant, *$P < 0.05$, **$P < 0.01$, ***$P < 0.001$ versus Control group.

a decrease in the SOD and GSH/GSSG levels in contrast to the Sham group, while the application of miR-342-5p mimic partly reversed such decrease (Figure 2E and F). These findings suggested that miR-342-5p mitigated oxidative stress of the brain tissue after cerebral ischemic/reperfusion in mice.

MiR-342-5p Inhibited RSL3-Induced Ferroptosis in MCAO/R Mice

Ferroptosis engages multiple pathways related to oxidative stress and antioxidant defense.[41] The functional enrichment analysis in Figure 1 further suggested the involvement of miR-342-5p in ferroptosis. Therefore, we proceeded to explore the in vivo correlation between miR-342-5p and ferroptosis. Targetscan online tool was utilized to predict the potential binding sites between miR-342-5p and ACSL4 (Figure 3A). The conducted dual-luciferase reporter assay demonstrated that the luciferase activity of the ACSL4 WT + miR-342-5p mimic group was observably impaired compared with the ACSL4 WT + NC mimic group, confirming the binding affinity between ACSL4 and miR-342-5p (Figure 3B). Injection of RSL3, the most potent inhibitor of GPX4, has been proven to effectively induce ferroptosis in previous studies.[42–44] Therefore, to investigate the effect of miR-342-5p on ferroptosis, the operated mice were injected with 30 mg/kg RSL3 based on the body weight. We examined both ACSL4 and Fe^{2+} levels and observed that treatment with RSL3 significantly elevated the contents of ACSL4 and Fe^{2+} in the MCAO/R mice, respectively. This funding indicates that RSL3 exacerbated ferroptosis of brain tissue induced by MCAO/R, while injection of miR-342-5p mimic partially reversed these changes (Figure 3C-E).

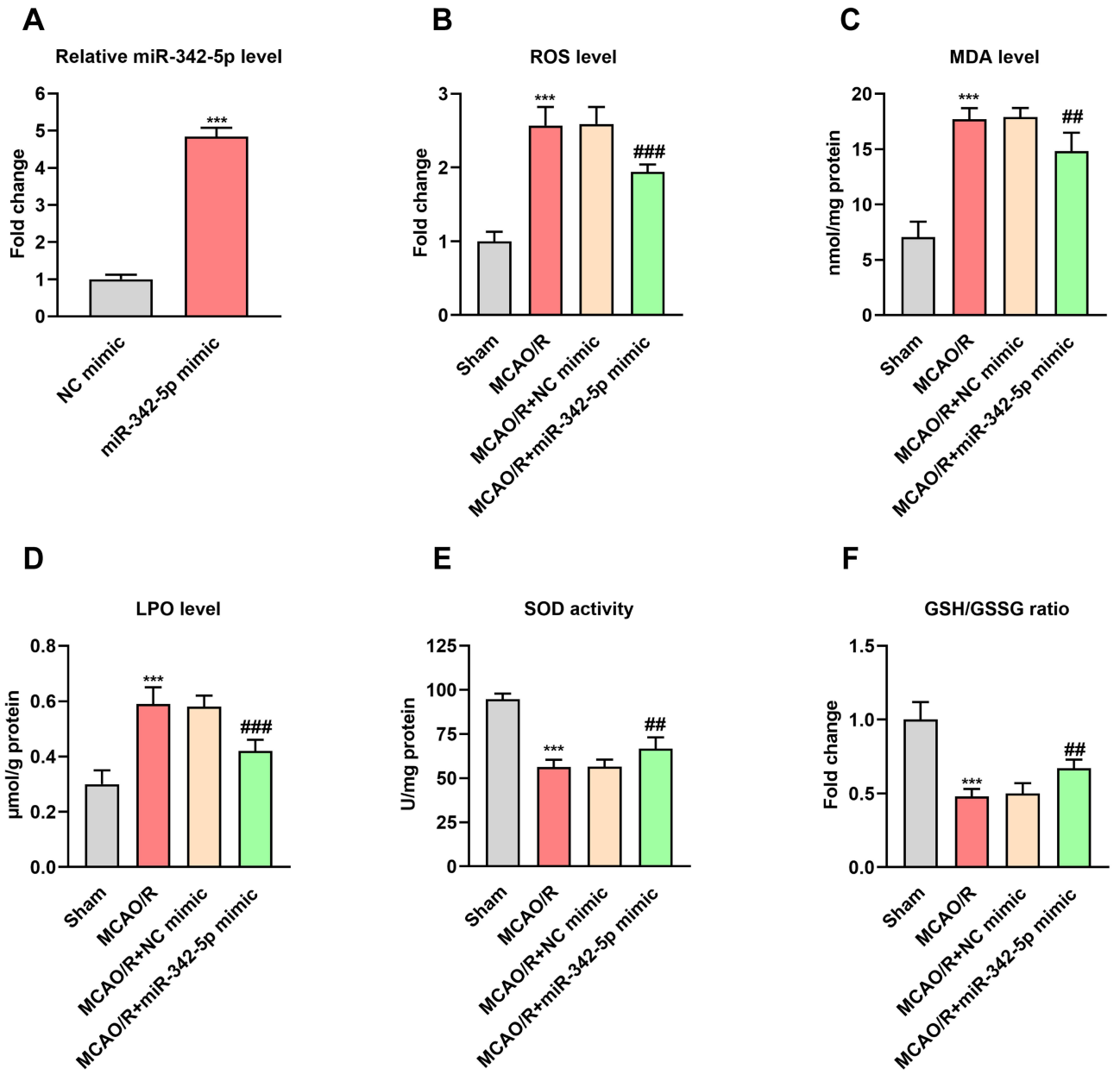

Figure 2 MiR-342-5p suppressed oxidative stress in MCAO/R mice. At 24 h post-modeling, the cortical tissues from each group were gathered to analyze the contents of miR-342-5p (**A**) using qRT-PCR (n = 6 per group). The ROS level (**B**), MDA level (**C**), LPO level (**D**), SOD activity (**E**) and GSH/GSSG ratio (**F**) were also measured using the corresponding detection kits (n = 6 per group). Results were expressed as mean ± SD of three independent experiments. $^{***}P < 0.001$ versus NC mimic group or Sham group; $^{\#\#}P < 0.01$, $^{\#\#\#}P < 0.001$ versus MCAO/R + NC mimic group.

In summary, the aforementioned results emphasized the capability of miR-342-5p in inhibiting ferroptosis following cerebral ischemic/reperfusion.

Targeting Association Between Circ_0008146 and miR-342-5p

Next, we tried to investigate the upstream mechanism regulating miR-342-5p expression in ischemic stroke. It is widely recognized that circRNAs may function as miRNA sponges, influencing miRNA levels according to the ceRNA hypothesis,[45] so circRNA and target miRNA usually demonstrate an opposite expression trend and biological function in certain diseases. A previous report showed that circ_0008146 was upregulated in MCAO/R mice and promoted apoptosis and neuroinflammation.[46] Considering the downregulation and beneficial effects of miR-342-5p in stroke conditions,

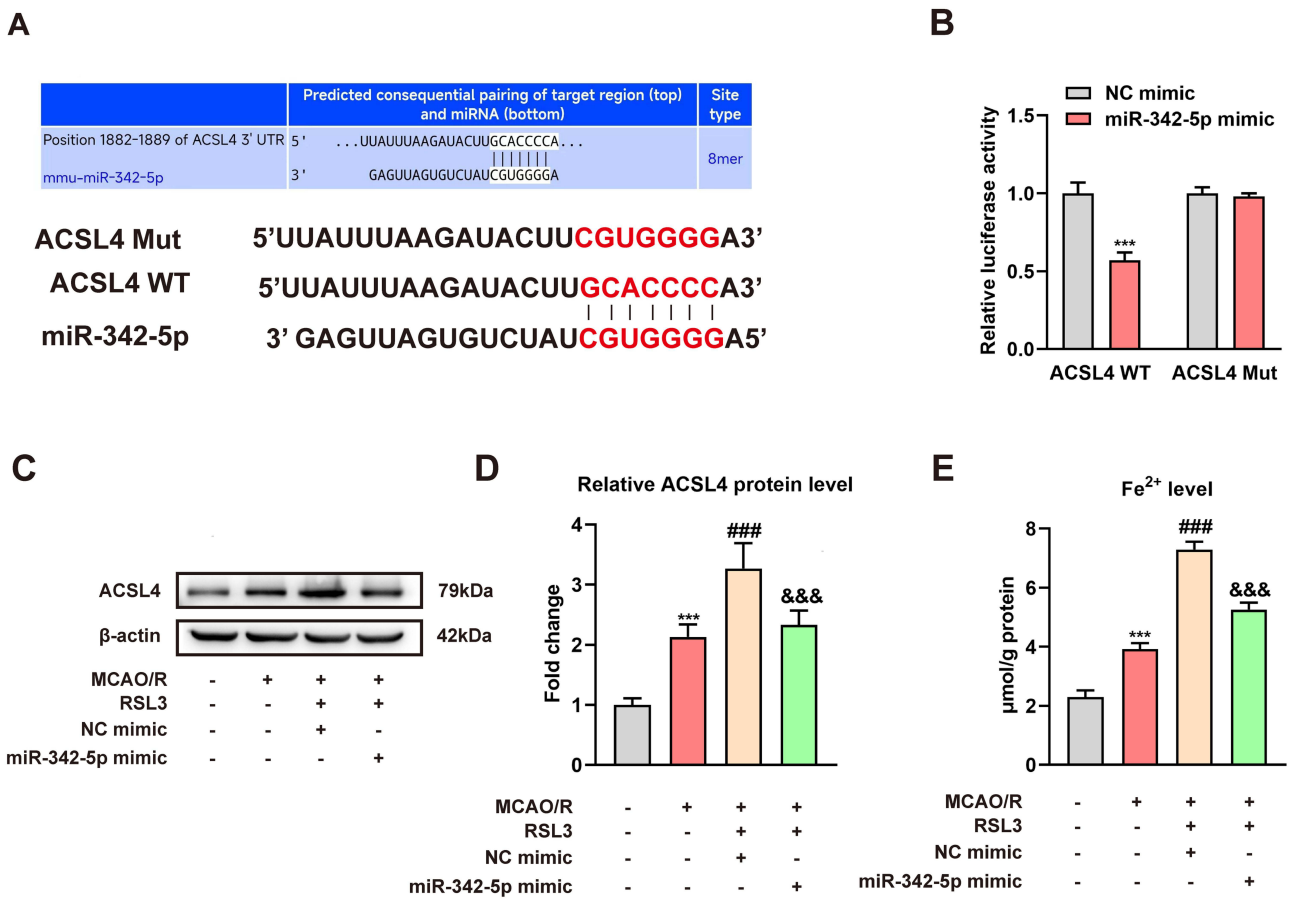

Figure 3 MiR-342-5p inhibited RSL3-induced ferroptosis in MCAO/R mice. (**A**) Putative biological targets between 3' UTR of ACSL4 mRNA and miR-342-5p using Targetscan. (**B**) Luciferase reporter assay shows relative luciferase activity of HEK 293T cells co-transfected with ACSL4WT or ACSL4 Mut and miR-342-5p mimic or NC mimic, respectively (n = 3 per group). (**C** and **D**) Typical Western blot images and quantification of ACSL4 protein levels in each group. β-actin was used as an internal control (n = 6 per group). (**E**) Fe^{2+} contents in each group were measured using iron assay kit (n = 6 per group). Results were expressed as mean ± SD of three independent experiments. $^{***}P < 0.001$ versus NC mimic group or Sham group; $^{\#\#\#}P < 0.001$ versus MCAO/R group; $^{\&\&\&}P < 0.001$ versus MCAO/R + RSL3 + NC mimic group.

circ_0008146 was selected and tested as a potential upstream circRNA in our successive studies. To assess the regulatory relationship between circ_0008146 and miR-342-5p, we employed RNAhybrid to speculate the potential binding sites, and the minimum free energy (mfe) is below −25 kcal/mol (Figure 4A). Subsequently, we conducted a luciferase reporter gene assay to verify the binding affinity of circ_0008146 to miR-342-5p. The luciferase activity of HEK 293T cells co-transfected with circ_0008146 WT and miR-342-5p mimic turned out to be lower than in cells co-transfected with NC mimic (Figure 4B). To confirm the in vivo effect of circ_0008146 on miR-342-5p, we overexpressed circ_0008146 in established MCAO/R models using lentiviral vectors. Subsequent qRT-PCR results verified the overexpression efficiency of circ_0008146 in MCAO/R mice (Figure 4C). Then, we found that the increased expression of circ_0008146 could lead to a reduction in miR-342-5p levels in the mouse brain tissues (Figure 4D). In view of these results, circ_0008146 may serve as a sponge of miR-342-5p and suppress the expression of miR-342-5p in MCAO/R mice.

Overexpression of Circ_0008146 Exacerbated Brain Infarction in MCAO/R Mice

The assessment of neurobehavioral function affected by the injection of circ_0008146 was conducted using the mNSS score, corner test, and rotarod test as previously described. Furthermore, circ_0008146 has been repeatedly suggested to be related to a bad outcome. Generally, the group treated with LV-circ_0008146 exhibited significantly higher neurological deficit scores, a higher number of right turns in the corner test and shorter latency time to fall in the rotarod test by contrast with LV-NC group (Figure 5A-C). The cerebral infarct volume was visualized using TTC staining. The stained brain tissues from the LV-circ_0008146 treated group exhibited a significantly larger infarct size ratio compared to those

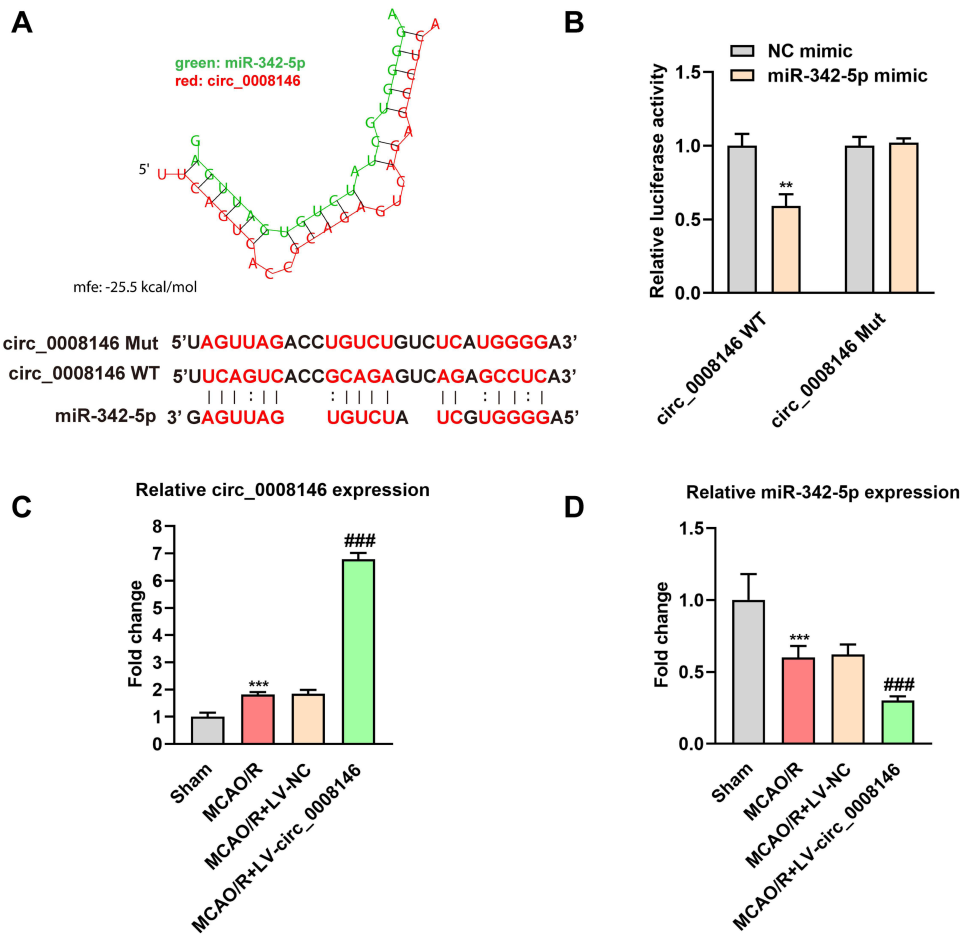

Figure 4 Targeting association between circ_0008146 and miR-342-5p. (**A**) Speculated targets between circ_0008146 and miR-342-5p using RNAhybrid (mfe: −25.5 kcal/mol). (**B**) Luciferase reporter assay shows relative luciferase activity of HEK 293T cells co-transfected with circ_0008146 WT or circ_0008146 Mut and miR-342-5p mimic or NC mimic (n = 3 per group). (**C** and **D**) Circ_0008146 and miR-342-5p content in each group was measured using qRT-PCR (n = 6 per group). Results were expressed as mean ± SD of three independent experiments. $^{**}P < 0.01$ versus NC mimic group; $^{***}P < 0.001$ versus Sham group; $^{\#\#\#}P < 0.001$ versus MCAO/R + LV-NC group.

from the LV-NC treated group (Figure 5D and E). Nissl staining was employed to detect histological changes and neuronal damage. The MCAO/R+LV-circ_0008146 group demonstrated more injured cells and neuronal loss compared to the MCAO/R+LV-NC group (Figure 5F). All these findings suggested that overexpression of circ_0008146 promoted brain injury in MCAO/R mice.

Circ_0008146 Contributed to Ferroptosis in Cerebral Infarction via Sponging miR-342-5p to Regulate ACSL4

Based on the above results, we attempted to further elucidate the role of the circ_0008146/miR-342-5p/ACSL4 axis on ischemic stroke. In the MCAO/R mice, the overexpression of circ_0008146 with lentiviral vectors resulted in increased levels of ROS, MDA and LPO, along with a decrease in SOD activity or GSH/GSSG ratio. However, the administration of miR-342-5p partially reversed these effects (Figure 6A-E). Similarly, circ_0008146 overexpressing promoted the iron accumulation in the mouse brain due to cerebral ischemic/reperfusion, whereas treatment with miR-342-5p partly attenuated the iron accumulation due to stroke (Figure 6F). As a promoter and marker of ferroptosis, ACSL4 was also evaluated through Western blot. As anticipated, the obtained outcomes unveiled an enhanced expression of the ACSL4 protein in the group administered with circ_0008146. However, treatment with miR-342-5p resulted in the down-regulation of ACSL4 protein levels compared to the group treated with circ_0008146 alone in MCAO/R mice

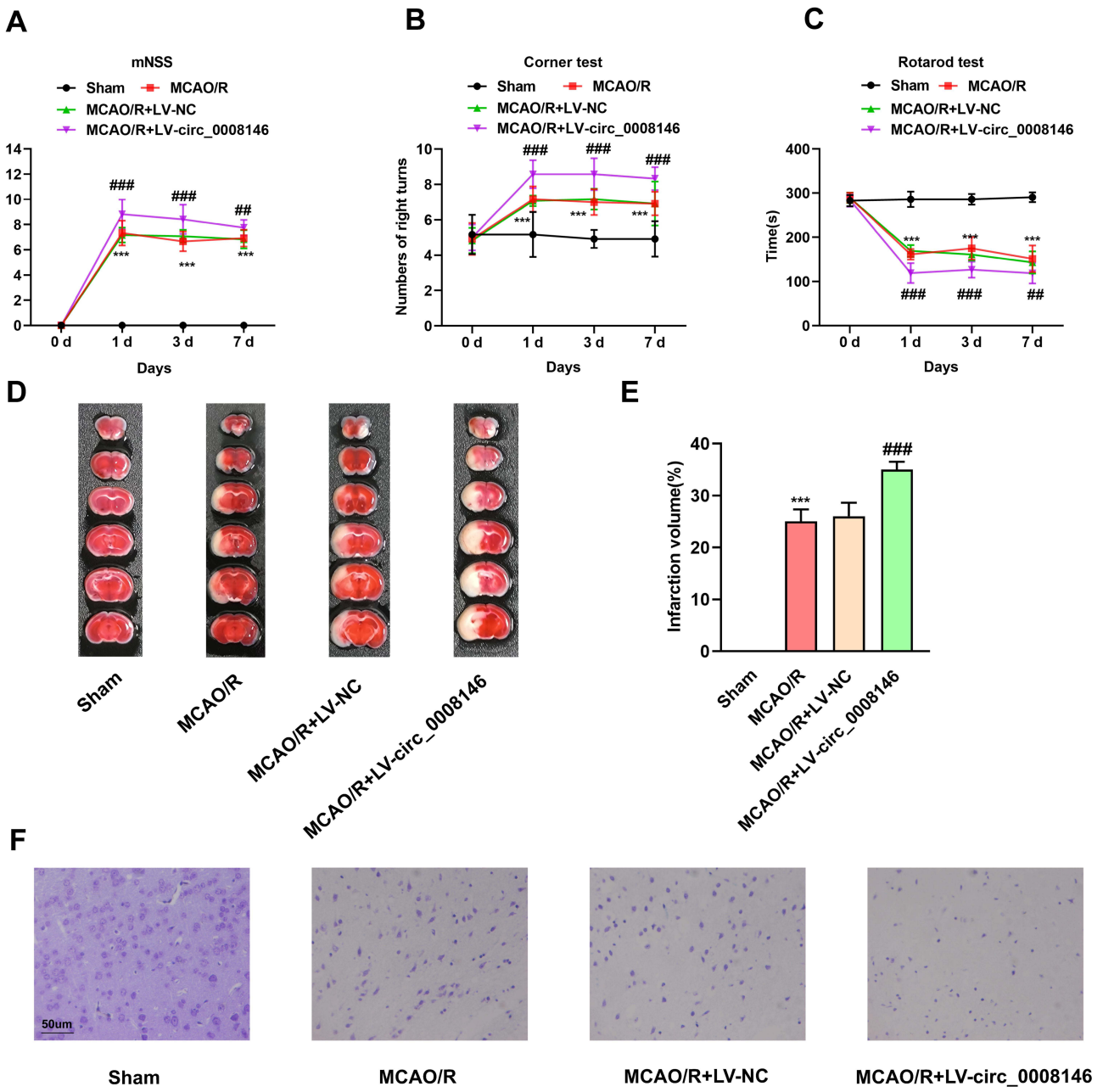

Figure 5 Overexpression of circ_0008146 exacerbated neurological deficit in MCAO/R mice. The mNSS score (**A**), corner test (**B**), and rotarod test (**C**) were performed at day 0, 1, 3, and 7 after MCAO/R operation to evaluate the neurobehavioral function (n = 12 per group). (**D** and **E**) The effects of circ_0008146 on infarct volume were evaluated by TTC staining at 7 days after reperfusion (n = 6 per group). (**F**) Typical images of Nissl staining for the ischemia-reperfusion area in cortex (n = 6 per group). Results were expressed as mean ± SD of three independent experiments. ***P < 0.001 MCAO/R group versus Sham group; ###P < 0.01, ####P < 0.001 MCAO/R + LV-circ_0008146 group versus MCAO/R + LV-NC group.

(Figure 6G and H). Taken together, these results revealed the possible regulation of circ_0008146/miR-342-5p/ACSL4 axis on ferroptosis in MCAO/R mice.

Hsa-miR-342-5p and ACSL4 Could Be Clinical Biomarker for AIS Patients

To investigate the clinical value of miR-342-5p/ACSL4 axis in diagnosing AIS, we recruited another 37 healthy controls and 32 AIS patients and measured the hsa-miR-342-5p levels and ACSL4 mRNA levels in their plasma by qRT-PCR. Consistent with Figure 1, plasma miR-342-5p levels in AIS participants were significant lower compared with the control group (Figure 7A). Also, ACSL4 mRNA levels were higher in the plasma of AIS patients than the healthy controls

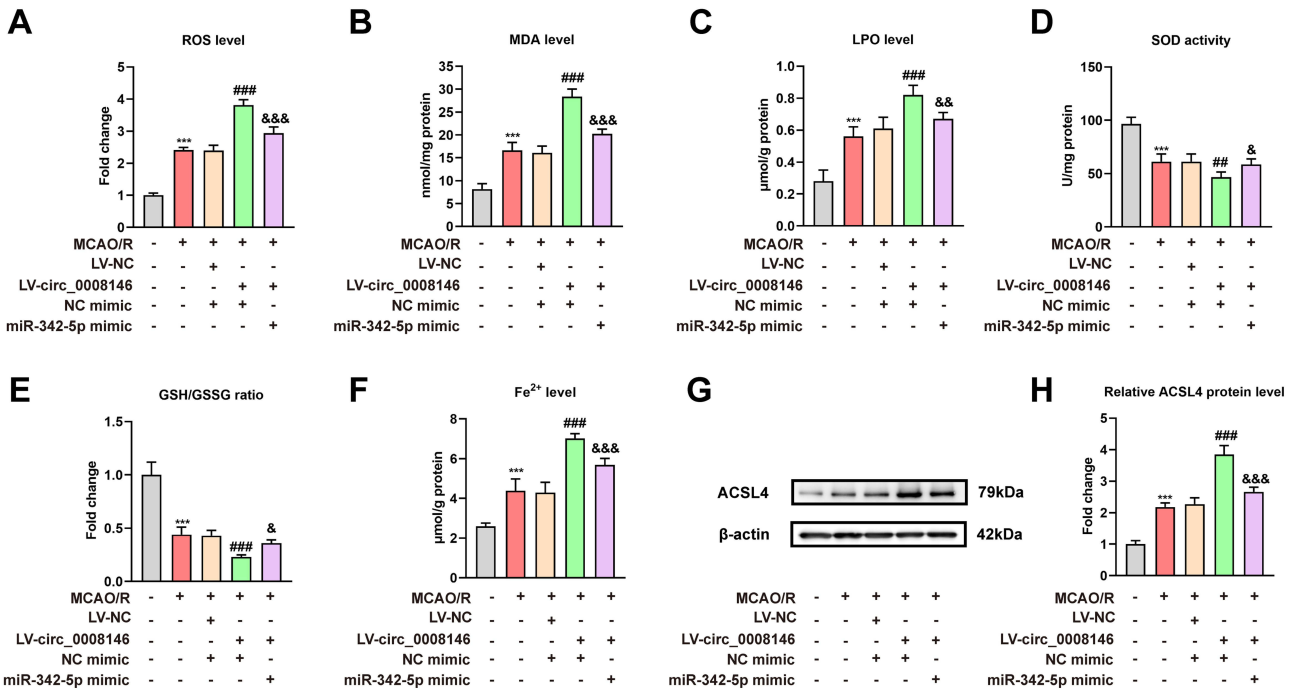

Figure 6 The circ_0008146/miR-342-5p/ACSL4 axis regulated ferroptosis in AIS induced by MCAO/R. ROS level (**A**), MDA level (**B**), LPO level (**C**), SOD activity (**D**), GSH/GSSG ratio (**E**) and Fe^{2+} level (**F**) of mouse brain tissues were measured using the corresponding detection kits (n = 6 per group). (**G** and **H**) Typical Western blot images and quantification of ACSL4 protein levels in each group. β-actin was used as an internal control (n = 6 per group). Results were expressed as mean ± SD of three independent experiments. $^{***}P < 0.001$ versus Sham group; $^{\#\#}P < 0.01$, $^{\#\#\#}P < 0.001$ versus MCAO/R + LV-NC + NC mimic group. $^{\&}P < 0.05$, $^{\&\&}P < 0.01$, $^{\&\&\&}P < 0.001$ versus MCAO/R + LV-circ_0008146 + NC mimic group.

(Figure 7B). ROC curves showed that both miR-342-5p (area under the curve, 0.786) and ACSL4 mRNA (area under the curve, 0.813) levels have a good ability to discriminate the AIS patients and healthy individuals (Figure 7C), demonstrating the potential of miR-342-5p and ACSL4 in diagnosing AIS. Interestingly, we found that in AIS patients, the plasma miR-342-5p levels were negatively correlated with the ACSL4 mRNA levels (Figure 7D), which revealed that the targeting relationship between miR-342-5p and ACSL4 may apply to AIS patients. Finally, we divided AIS patients into two groups according to stroke severity evaluated by National Institutes of Health Stroke Scale (NIHSS) score: mild group (NIHSS < 5) and moderate to severe group (NIHSS ≥ 5), and compared the levels of miR-342-5p and ACSL4 mRNA in these two groups. As shown in Figure 7E and F, miR-342-5p in plasma was relatively lower in moderate to severe group than mild group, whereas the moderate to severe group has higher ACSL4 mRNA plasma levels. In general, these clinical results indicated the potential of miR-342-5p and ACSL4 as diagnostic markers and therapeutic targets for AIS patients.

Discussion

AIS is characterized by a high rate of disability and mortality, while there is still a significant unmet need for treatment of the large AIS population.[47,48] MiRNAs belong to small, non-coding RNA molecules and are found to be important in the regulation of gene expression after transcription.[16] Most of miRNAs are involved in regulating mRNA through its degradation, in addition to controlling protein expression.[18] In very recent times, a large number of miRNAs were detected and speculated to serve as potential therapeutic targets for AIS.[17] For example, it was found that activating miR-337-3p/Nampt exerted neuroprotective effects.[32] Exogenous miRNA-181b could activate the PTEN/Akt signal pathway and promoted angiogenesis, alleviating neuronal damage in ischemic stroke.[49] Moreover, blood miRNAs are good predictors of stroke risk.[50] Herein, we conducted small RNA sequencing and qRT-PCR analysis and detected the pronounced downregulated miRNA, hsa-miR-342-5p. This finding was consistent with previous studies, which demonstrated that miR-342-5p was significantly downregulated in both MCAO/R mice and OGD/R cells. Also, miR-342-5p has

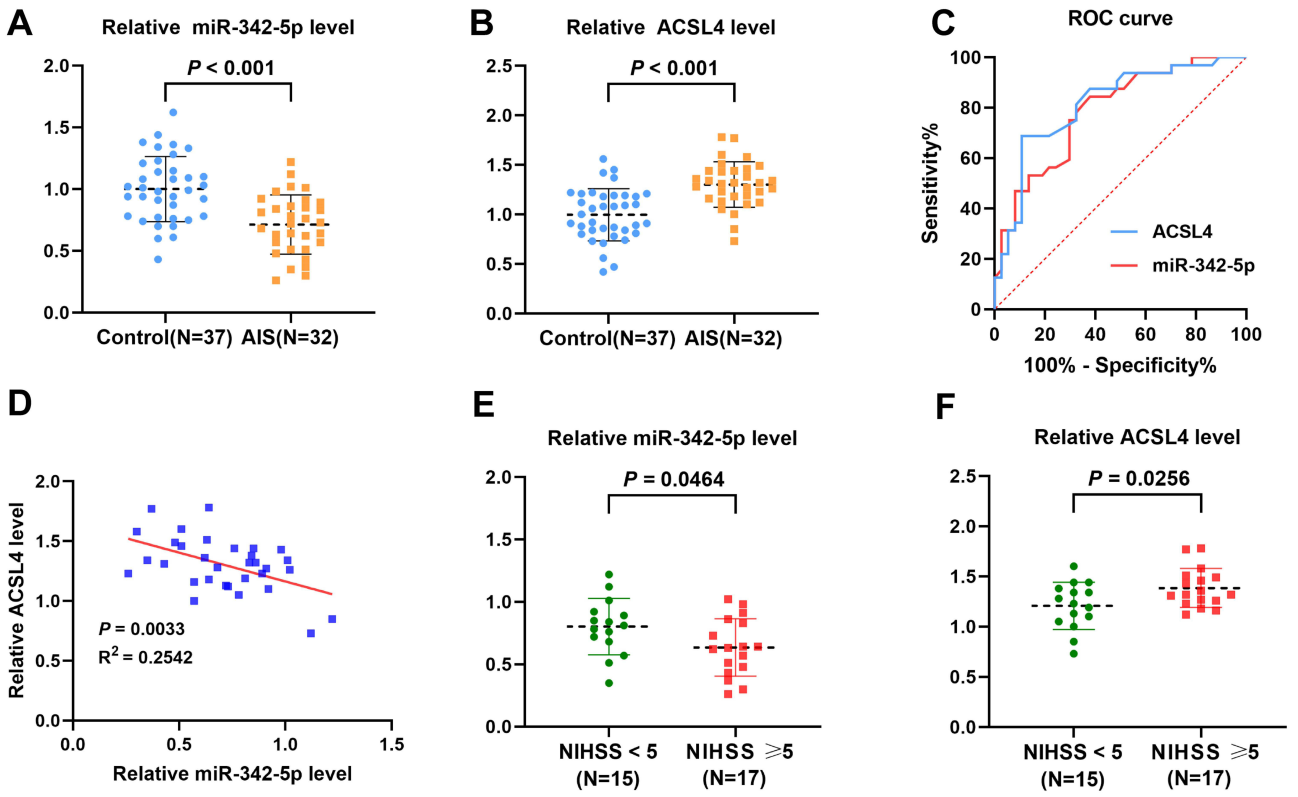

Figure 7 Hsa-miR-342-5p and ACSL4 in the plasma could be clinical biomarker for AIS. (**A** and **B**) MiR-342-5p and ACSL4 mRNA levels were measured in the plasma of 37 healthy controls and 32 AIS patients using qRT-PCR. (**C**) ROC curves demonstrated the diagnostic value of miR-342-5p and ACSL4 for AIS. (**D**) The negative correlation between miR-342-5p and ACSL4 mRNA in the plasma of the 32 AIS patients detected by qRT-PCR. (**E** and **F**) The 32 AIS patients were divided into mild group (NIHSS < 5) and moderate to severe group (NIHSS ≥ 5), and miR-342-5p or ACSL4 mRNA levels were measured in the plasma using qRT-PCR. Results were expressed as mean ± SD.

shown a protective effect against neuronal apoptosis.[36,51] Nevertheless, the functions and mechanisms of miR-342-5p in AIS have been relatively underexplored.

Featured with increased metabolic activity and susceptibility to ischemic stroke, brain is prone to suffer from oxidative damage.[52] Substantial evidence suggests that oxidative stress exerts a negative influence on AIS and subsequent reperfusion injury.[37,51,53] In a study on lung injury, miR-342 inhibited oxidative stress in human bronchial epithelial cells by targeting KLF5, suggesting inhibition of oxidative stress may also be the mechanism by which miR-342-5p exerts its neuroprotective effect in AIS.[54] In our study, we discovered that attenuated oxidative stress and ameliorated neurological deficits were a reflection of increased miR-342-5p. This positive effect of miR-342-5p on AIS is consistent with the earlier findings. Oxidative stress has been reported to correlate with ferroptotic responses, and furthermore, the accumulation of lipid peroxides serves as a biochemical signature of ferroptosis.[41] Considering the crosstalk between oxidative stress and ferroptosis, we focused on the effect of miR-342-5p on ferroptosis using ferroptosis inducer, and discovered that miR-342-5p inhibited RSL3-induced ferroptosis in MCAO/R mice. To the best of our knowledge, this is the first study connecting miR-342-5p and ferroptosis with cerebral ischemia. As a direct target of miR-342-5p, ACSL4 is involved in intracellular synthesis of lipid peroxide substrates and is considered to be a classic marker of ferroptosis.[55] We verified the negative correlation between miR-342-5p and ACSL4 in AIS patients, and found that miR-342-5p and ACSL4 have good diagnostic value for AIS. The different expression of miR-342-5p and ACSL4 in mild and moderate to severe groups also suggests that regulation of miR-342-5p/ACSL4 may be a potential therapeutic approach for AIS.

Considering the effect of miRNA dysregulation on ischemia-reperfusion injury, it is necessary to explore the upstream mechanism of miR-342-5p expression. In recent years, the circRNA/miRNA sponging mechanism theory proposes that circRNAs could competitively bind to miRNAs, thereby preventing miRNA interaction with mRNA

targets. There is mounting evidence indicating that circRNAs are engaged in regulating pathophysiological processes of ischemic stroke by acting as miRNA sponges.[56–58] For example, circZfp609 promotes OGD/R-induced astrocyte injury by influencing BACH1 expression through sponging miR-145a-5p.[59] Also, circDLGAP4 was reported to sponge miR-143 in endothelial cells, and reduce the blood-brain barrier damage caused by ischemic stroke.[60] In the previous study by Li et al, circ_0008146 was identified as upregulated in the cerebral cortex of MCAO/R mice, and its expression significantly decreased after treatment. Initial cell experiments suggest its involvement in inflammation and apoptosis promotion. Therefore, we suspected that circ_0008146 is upstream of miR-342-5p regulation, which was validated in our study.[46] In fact, circRNAs are key factors in influencing the risk of oxidative-stress-related diseases.[61–63] In our study, we identified that the overexpression of circ_0008146 exacerbated cerebral infarction and impaired functional behavior, which is the first time to validate the detrimental effect of circ_0008146 on stroke in an in vivo model. Moreover, ferroptosis may be a key pathological process through which circ_0008146 exacerbates cerebral ischemia-reperfusion injury. Despite the limited research on circ_0008146, our study provided a potential direction for more detailed mechanistic studies in the future.

Some limitations must be acknowledged in our study. Firstly, the sample size of both normal controls and AIS patients is relatively small. Hence, our results need to be confirmed with a larger cohort in future studies. Secondly, our experiments were mainly conducted on animal models, which can more accurately simulate the complex environment in vivo, but we did not perform cellular experiments to further explore and validate the mechanisms involved. We plan to design and conduct such experiments to address this aspect in subsequent research. Thirdly, in our study, ACSL4 is considered to be the key protein in which miR-342-5p exerts ferroptosis inhibition, but considering the complex regulatory mechanism of ferroptosis related genes, whether miR-342-5p exerts its role through other proteins related to ferroptosis remains to be further investigated.

Conclusion

Our study provided evidence that the administration of miR-342-5p can effectively mitigate brain damage resulting from ferroptosis. Furthermore, our study elucidated the underlying mechanism of circ_0008146 on exacerbating neuronal damage after AIS via the circ_0008146/miR-342-5p/ACSL4 axis. These findings suggest that such an axis holds promise as an available and practical therapeutic focus in AIS.

Data Sharing Statement

The data that support this study are available from the corresponding author Rui Duan upon reasonable request.

Ethical Approval

This study was in full compliance with the Declaration of Helsinki and was approved by the Ethics Committee of Nanjing First Hospital, Nanjing Medical University (No. KY20211011-05). All study participants provided written informed consent before enrollment in the study. This study was also approved by the Laboratory Animal Ethics Committee of Nanjing First Hospital, Nanjing Medical University (No. DWSY-23146450). The experimental protocol was conducted in accordance with the Guide for the Care and Use of Laboratory Animals of the National Institutes of Health.

Author Contributions

All authors made a significant contribution to the work reported, whether that is in the conception, study design, execution, acquisition of data, analysis and interpretation, or in all these areas; took part in drafting, revising or critically reviewing the article; gave final approval of the version to be published; have agreed on the journal to which the article has been submitted; and agree to be accountable for all aspects of the work.

Funding

This study was funded by Jiangsu Provincial Medical Key Discipline Cultivation Unit (JSDW202239) and Key Project supported by Medical Science and technology development Foundation, Nanjing Department of Health (YKK22107).

Disclosure

The authors report no conflicts of interest in this work.

References

1. Claassen J, Thijssen DHJ, Panerai RB, Faraci FM. Regulation of cerebral blood flow in humans: physiology and clinical implications of autoregulation. Physiol Rev. 2021;101(4):1487–1559. doi:10.1152/physrev.00022.2020
2. Walter K. What is acute ischemic stroke? *JAMA*. 2022;327(9):885. doi:10.1001/jama.2022.1420
3. Shi K, Tian DC, Li ZG, Ducruet AF, Lawton MT, Shi FD. Global brain inflammation in stroke. *Lancet Neurol*. 2019;18(11):1058–1066.
4. Hu Q, Zhou Q, Wu J, Wu X, Ren J. The role of mitochondrial DNA in the development of ischemia reperfusion injury. *Shock*. 2019;51(1):52–59. doi:10.1097/SHK.0000000000001190
5. Liu S, Feng X, Jin R, Li G. Tissue plasminogen activator-based nanothrombolysis for ischemic stroke. *Expert Opin Drug Deliv*. 2018;15 (2):173–184. doi:10.1080/17425247.2018.1384464
6. Hacke W, Kaste M, Bluhmki E, et al. Thrombolysis with alteplase 3 to 4.5 hours after acute ischemic stroke. *N Engl J Med*. 2008;359 (13):1317–1329. doi:10.1056/NEJMoa0804656
7. Han B, Zhang Y, Zhang Y, et al. Novel insight into circular RNA HECTD1 in astrocyte activation via autophagy by targeting MIR142-TIPARP: implications for cerebral ischemic stroke. *Autophagy*. 2018;14(7):1164–1184. doi:10.1080/15548627.2018.1458173
8. Wang L, Liu Y, Zhang X, et al. Endoplasmic reticulum stress and the unfolded protein response in cerebral ischemia/reperfusion injury. *Front Cell Neurosci*. 2022;16:864426. doi:10.3389/fncel.2022.864426
9. Ward RJ, Zucca FA, Duyn JH, Crichton RR, Zecca L. The role of iron in brain ageing and neurodegenerative disorders. *Lancet Neurol*. 2014;13 (10):1045–1060. doi:10.1016/S1474-4422(14)70117-6
10. Lu J, Xu F, Lu H. LncRNA PVT1 regulates ferroptosis through miR-214-mediated TFR1 and p53. *Life Sci*. 2020;260:118305. doi:10.1016/j.lfs.2020.118305
11. Li J, Cao F, Yin HL, et al. Ferroptosis: past, present and future. *Cell Death Dis*. 2020;11(2):88. doi:10.1038/s41419-020-2298-2
12. Yu Y, Yan Y, Niu F, et al. Ferroptosis: a cell death connecting oxidative stress, inflammation and cardiovascular diseases. *Cell Death Discov*. 2021;7 (1):193. doi:10.1038/s41420-021-00579-w
13. Tang D, Chen X, Kang R, Kroemer G. Ferroptosis: molecular mechanisms and health implications. *Cell Res*. 2021;31(2):107–125. doi:10.1038/s41422-020-00441-1
14. Li D, Li Y. The interaction between ferroptosis and lipid metabolism in cancer. *Signal Transduct Target Ther*. 2020;5(1):108. doi:10.1038/s41392-020-00216-5
15. Cui Y, Zhang Y, Zhao X, et al. ACSL4 exacerbates ischemic stroke by promoting ferroptosis-induced brain injury and neuroinflammation. *Brain Behav Immun*. 2021;93:312–321. doi:10.1016/j.bbi.2021.01.003
16. Saliminejad K, Khorram khorshid HR, Soleymani Fard S, Ghaffari SH. An overview of microRNAs: biology, functions, therapeutics, and analysis methods. *J Cell Physiol*. 2019;234(5):5451–5465. doi:10.1002/jcp.27486
17. Toor SM, Aldous EK, Parray A, et al. Circulating MicroRNA profiling identifies distinct microRNA signatures in acute ischemic stroke and transient ischemic attack patients. *Int J Mol Sci*. 2022;24(1):108. doi:10.3390/ijms24010108
18. Condrat CE, Thompson DC, Barbu MG, et al. miRNAs as biomarkers in disease: latest findings regarding their role in diagnosis and prognosis. *Cells*. 2020;9(2): 276.
19. Lindholm EM, Leivonen SK, Undlien E, et al. miR-342-5p as a potential regulator of HER2 breast cancer cell growth. *microRNA*. 2019;8 (2):155–165. doi:10.2174/2211536608666181206124922
20. Sun X, Wu Y, Gu M, Zhang Y. miR-342-5p decreases ankyrin G levels in Alzheimer's disease transgenic mouse models. *Cell Rep*. 2014;6 (2):264–270. doi:10.1016/j.celrep.2013.12.028
21. Hou Z, Qin X, Hu Y, et al. Longterm exercise-derived exosomal miR-342-5p: a novel exerkine for cardioprotection. *Circ Res*. 2019;124 (9):1386–1400. doi:10.1161/CIRCRESAHA.118.314635
22. Misir S, Wu N, Yang BB. Specific expression and functions of circular RNAs. *Cell Death Differ*. 2022;29(3):481–491.
23. Jeck WR, Sharpless NE. Detecting and characterizing circular RNAs. *Nat Biotechnol*. 2014;32(5):453–461. doi:10.1038/nbt.2890
24. Zhang X, Wan M, Min X, et al. Circular RNA as biomarkers for acute ischemic stroke: a systematic review and meta-analysis. *CNS Neurosci Ther*. 2023;29(8):2086–2100. doi:10.1111/cns.14220
25. Song Y, Zhang L, Liu X, et al. Analyses of circRNA profiling during the development from pre-receptive to receptive phases in the goat endometrium. *J Anim Sci Biotechnol*. 2019;10:34.
26. Li H, Shan C, Wang J, Hu C. CircRNA Hsa_circ_0001017 inhibited gastric cancer progression via acting as a sponge of miR-197. *Dig Dis Sci*. 2021;66(7):2261–2271. doi:10.1007/s10620-020-06516-8
27. Zhou Y, Liu Y, Kang Z, et al. CircEPS15, as a sponge of MIR24-3p ameliorates neuronal damage in Parkinson disease through boosting PINK1-PRKN-mediated mitophagy. *Autophagy*. 2023;19(9):2520–2537. doi:10.1080/15548627.2023.2196889
28. Liu Y, Huang Y, Zhang X, et al. CircZXDC promotes vascular smooth muscle cell transdifferentiation via regulating miRNA-125a-3p/ABCC6 in moyamoya disease. *Cells*. 2022;11(23): 3792.
29. Xie H, Huang Y, Zhan Y. Construction of a novel circRNA-miRNA-ferroptosis related mRNA network in ischemic stroke. *Sci Rep*. 2023;13 (1):15077. doi:10.1038/s41598-023-41028-1
30. Dankbaar JW, Bienfait HP, van den Berg C, et al. Wake-up stroke versus stroke with known onset time: clinical and multimodality ct imaging characteristics. *Cerebrovascular Dis*. 2018;45(5–6):236–244. doi:10.1159/000489566
31. Evenson KR, Rosamond WD, Vallee JA, Morris DL. Concordance of stroke symptom onset time. The second delay in accessing stroke healthcare (DASH II) study. *Ann Epidemiol*. 2001;11(3):202–207. doi:10.1016/S1047-2797(00)00211-8
32. Hu J, Duan H, Zou J, et al. METTL3-dependent N6-methyladenosine modification is involved in berberine-mediated neuroprotection in ischemic stroke by enhancing the stability of NEAT1 in astrocytes. *Aging*. 2024;15: 299.

33. Chen J, Yang L, Geng L, et al. Inhibition of acyl-CoA synthetase long-chain family member 4 facilitates neurological recovery after stroke by regulation ferroptosis. *Front Cell Neurosci*. 2021;15:632354. doi:10.3389/fncel.2021.632354
34. Du Y, Zhang R, Zhang G, Wu H, Zhan S, Bu N. Downregulation of ELAVL1 attenuates ferroptosis-induced neuronal impairment in rats with cerebral ischemia/reperfusion via reducing DNMT3B-dependent PINK1 methylation. *Metab Brain Dis*. 2022;37(8):2763–2775. doi:10.1007/s11011-022-01080-8
35. Wang X, Xia P, Song J, et al. Cranial electrotherapy stimulation alleviates depression-like behavior of post-stroke depression rats by upregulating GPX4-mediated BDNF expression. *Behav. Brain Res*. 2023;437:114117. doi:10.1016/j.bbr.2022.114117
36. Yu Z, Zhu M, Shu D, et al. LncRNA PEG11as aggravates cerebral ischemia/reperfusion injury after ischemic stroke through miR-342-5p/PFN1 axis. *Life Sci*. 2023;313:121276. doi:10.1016/j.lfs.2022.121276
37. Puzio M, Moreton N, O'Connor JJ. Neuroprotective strategies for acute ischemic stroke: targeting oxidative stress and prolyl hydroxylase domain inhibition in synaptic signalling. *Brain Disorders*. 2022;5: 100030.
38. Zhao Y, Zhang X, Chen X, Wei Y. Neuronal injuries in cerebral infarction and ischemic stroke: from mechanisms to treatment (review). *Int J Mol Med*. 2022;49(2): 1–9.
39. Sun YY, Zhu HJ, Zhao RY, et al. Remote ischemic conditioning attenuates oxidative stress and inflammation via the Nrf2/HO-1 pathway in MCAO mice. *Redox Biol*. 2023;66:102852. doi:10.1016/j.redox.2023.102852
40. Guo XH, Pang L, Gao CY, Meng FL, Jin W. Lyoniresinol attenuates cerebral ischemic stroke injury in MCAO rat based on oxidative stress suppression via regulation of Akt/GSK-3β/Nrf2 signaling. *Biomed Pharmacothe*. 2023;167:115543. doi:10.1016/j.biopha.2023.115543
41. Kuang F, Liu J, Tang D, Kang R. Oxidative damage and antioxidant defense in ferroptosis. *Front Cell Dev Biol*. 2020;8:586578. doi:10.3389/fcell.2020.586578
42. Zheng C, Wang C, Sun D, et al. Structure-activity relationship study of RSL3-based GPX4 degraders and its potential noncovalent optimization. *Eur J Med Chem*. 2023;255:115393. doi:10.1016/j.ejmech.2023.115393
43. Li X, Chen J, Feng W, et al. Berberine ameliorates iron levels and ferroptosis in the brain of 3 × Tg-AD mice. *Phytomedicine*. 2023;118:154962. doi:10.1016/j.phymed.2023.154962
44. Li S, He Y, Chen K, et al. RSL3 drives ferroptosis through NF-κB pathway activation and GPX4 depletion in glioblastoma. *Oxid Med Cell Longev*. 2021;2021:2915019. doi:10.1155/2021/2915019
45. Wu C, Du M, Yu R, et al. A novel mechanism linking ferroptosis and endoplasmic reticulum stress via the circPtpn14/miR-351-5p/5-LOX signaling in melatonin-mediated treatment of traumatic brain injury. *Free Radic Biol Med*. 2022;178:271–294. doi:10.1016/j.freeradbiomed.2021.12.007
46. Li L, Zhang D, Yao W, et al. Ligustrazine exerts neuroprotective effects via circ_0008146/miR-709/Cx3cr1 axis to inhibit cell apoptosis and inflammation after cerebral ischemia/reperfusion injury. *Brain Res Bull*. 2022;190:244–255. doi:10.1016/j.brainresbull.2022.10.011
47. Pu L, Wang L, Zhang R, Zhao T, Jiang Y, Han L. Projected global trends in ischemic stroke incidence, deaths and disability-adjusted life years from 2020 to 2030. *Stroke*. 2023;54(5):1330–1339. doi:10.1161/STROKEAHA.122.040073
48. Herpich F, Rincon F. Management of acute ischemic stroke. *Crit Care Med*. 2020;48(11):1654–1663. doi:10.1097/CCM.0000000000004597
49. Xue LX, Shu LY, Wang HM, et al. miR-181b promotes angiogenesis and neurological function recovery after ischemic stroke. *Neural Regen Res*. 2023;18(9):1983–1989. doi:10.4103/1673-5374.367957
50. Sonoda T, Matsuzaki J, Yamamoto Y, et al. Serum MicroRNA-based risk prediction for stroke. *Stroke*. 2019;50(6):1510–1518. doi:10.1161/STROKEAHA.118.023648
51. Elsayed WM, Abdel-Gawad E-HA, Mesallam DIA, El-Serafy TS. The relationship between oxidative stress and acute ischemic stroke severity and functional outcome. *Egypt J Neurol Psychiatry Neurosurg*. 2020;56(1). doi:10.1186/s41983-020-00206-y
52. Jelinek M, Jurajda M, Duris K. Oxidative stress in the brain: basic concepts and treatment strategies in stroke. *Antioxidants*. 2021;10(12):1886. doi:10.3390/antiox10121886
53. Kollar B, Siarnik P, Konarikova K, et al. The interplay of dyslipidemia, oxidative stress, and clinical outcomes in acute ischemic stroke patients with and without coronary artery disease. *Biomedicines*. 2024;12(2):332. doi:10.3390/biomedicines12020332
54. Zheng F, Liu T, Zhu J, Xie Y, Wu L, Lin Z. FoxF1 protects rats from paraquat-evoked lung injury following HDAC2 inhibition via the microRNA-342/KLF5/IκB/NF-κB p65 axis. *Exp. Cell. Res*. 2020;395(2):112208. doi:10.1016/j.yexcr.2020.112208
55. Ding K, Liu C, Li L, et al. Acyl-CoA synthase ACSL4: an essential target in ferroptosis and fatty acid metabolism. *Chin Med J*. 2023;136(21):2521–2537. doi:10.1097/CM9.0000000000002533
56. Liu Y, Li Y, Zang J, et al. CircOGDH is a penumbra biomarker and therapeutic target in acute ischemic stroke. *Circ Res*. 2022;130(6):907–924. doi:10.1161/CIRCRESAHA.121.319412
57. Liu M, Liu X, Zhou M, Guo S, Sun K. Impact of CircRNAs on ischemic stroke. *Aging Dis*. 2022;13(2):329–339. doi:10.14336/AD.2021.1113
58. Min X, Liu DL, Xiong XD. Circular RNAs as competing endogenous RNAs in cardiovascular and cerebrovascular diseases: molecular mechanisms and clinical implications. *Front Cardiovasc Med*. 2021;8:682357. doi:10.3389/fcvm.2021.682357
59. Zhou Z, Wang X, Hu Q, Yang Z. CircZfp609 contributes to cerebral infarction via sponging miR-145a-5p to regulate BACH1. *Metab Brain Dis*. 2023;38(6):1971–1981. doi:10.1007/s11011-023-01208-4
60. Bai Y, Zhang Y, Han B, et al. Circular RNA DLGAP4 ameliorates ischemic stroke outcomes by targeting miR-143 to regulate endothelial-mesenchymal transition associated with blood-brain barrier integrity. *J Neurosci*. 2018;38(1):32–50. doi:10.1523/JNEUROSCI.1348-17.2017
61. Zhang Y, Chen Y, Wan Y, et al. Circular RNAs in the regulation of oxidative stress. *Front Pharmacol*. 2021;12:697903. doi:10.3389/fphar.2021.697903
62. Chen Z, Huang Y, Chen Y, et al. CircFNDC3B regulates osteoarthritis and oxidative stress by targeting miR-525-5p/HO-1 axis. *Commun Biol*. 2023;6(1):200. doi:10.1038/s42003-023-04569-9
63. Wang Y, He W, Ibrahim SA, He Q, Jin J. Circular RNAs: novel players in the oxidative stress-mediated pathologies, biomarkers, and therapeutic targets. *Oxid Med Cell Longev*. 2021;2021:6634601. doi:10.1155/2021/6634601